photonics

MDPI

Article

Transmission Characteristics and Coupling Mechanisms of Gaussian Beams Under Combined Scattering and Turbulence Effects

Liguo Wang, Yue Yu, Lei Gong *, Wanjun Wang, Zhiqiang Yang, Lihong Yang and Yao Li

School of Opto-Electronical Engineering, Xi'an Technological University, Xi'an 710121, China; wangliguo@xatu.edu.cn (L.W.); yuyueasiapacific@126.com (Y.Y.); wangwanjun@xatu.edu.cn (W.W.); yangzhiqiang@xatu.edu.cn (Z.Y.); yanglihong@xatu.edu.cn (L.Y.); liyao@xatu.edu.cn (Y.L.)
* Correspondence: gonglei@xatu.edu.cn

Abstract

Atmospheric laser beam propagation is typically perturbed by the dual influences of aerosol particle systems and atmospheric turbulence. This joint perturbation induces intensity fluctuations in the transmitted optical field, which significantly degrades the performance of laser-based systems. This study integrates and improves upon existing simulation algorithms, establishing a coupled model that combines the Monte Carlo method and multi-phase screens. The model accurately characterizes optical field evolution and reveals that the impacts of scattering and turbulence on the scintillation index (SI) are not simply additive: turbulence perturbation enhances intensity fluctuations, leading to an increase in SI; however, as the energy proportion of scattered light rises, its statistical stationarity begins to dominate the optical field characteristics, stabilizing SI. Based on radiative transfer and Mie scattering theories, an analytical formula for single-scattering SI is derived, enabling direct calculation from fundamental parameters. Furthermore, a composite SI expression is established using the scattered-to-transmitted light intensity ratio. To address model deviations along the dimensions of visibility and turbulence strength, a sinusoidal compensation model and a logarithmic compensation model are proposed, respectively. Validation results verify the complementary and competitive mechanisms of scattering and turbulence in modulating intensity fluctuations. This research provides efficient theoretical tools and practical references for simulating and optimizing laser transmission in complex atmospheric environments.

Keywords: laser transmission; particle scattering–turbulence coupling; scintillation index

Received: 3 March 2026
Revised: 22 March 2026
Accepted: 24 March 2026
Published: 26 March 2026

1. Introduction

Lasers, as ideal information carriers, exhibit remarkable potential in optical communication, remote sensing, and lidar systems, thanks to their large bandwidth, electromagnetic interference immunity, and high transmission rates [1–3]. However, laser beam propagation through complex media is subject to joint perturbations from particle scattering and turbulence, leading to severe-intensity fluctuations, phase distortions, and energy attenuation that degrade transmission link stability and reliability [4–6]. Establishing an accurate simulation model for laser transmission under combined particle-turbulence effects, as well as clarifying the underlying influence mechanisms, is therefore critical for optimizing system design and enhancing performance in complex environments.

Light transport in discrete particle systems is a classic research topic, with the Monte Carlo (MC) method being the most widely used approach. By simulating stochastic photon–medium interaction processes, it effectively characterizes the randomness of light propagation [7–9]. The scalar MC algorithm, initially proposed for light transport in layered tissues [10], was later upgraded to vector methods to quantify polarization evolution after multiple scattering events [11]. In atmospheric scattering research, scalar methods have been applied to investigate laser attenuation, backscattering, and transmittance in fog and aerosols [12,13], while vector methods have enabled studies on polarized light transport, including size-dependent transmission or reflection of sea fog particles and polarization maintenance in foggy environments [14,15]. Phase screen theory is now extensively used in electromagnetic wave propagation research, covering laser and microwave transmission [16–18]. Early studies laid the groundwork for turbulent phase screen applications by analyzing the scintillation index of received intensity under different apertures [19]. Subsequent work focused on method optimization and scenario expansion: novel interpolation methods were proposed to improve dynamic simulation continuity [20], aperture effects on partially coherent beam SI were explored [21], and phase screen simulation efficiency, accuracy, and noise suppression were enhanced via high-frequency filtering, wavelet analysis, and refined low-frequency sampling [22–24]. Additionally, phase screen methods have been extended to high-power laser propagation and multi-aperture reception scenarios, enabling integrated simulation frameworks accounting for multiple physical effects [25,26].

Nevertheless, the MC method cannot accurately simulate turbulence-induced random phase fluctuations, whereas the phase screen method fails to capture dynamic energy ratio variations between scattered and transmitted light. This necessitates the development of a hybrid model incorporating both mechanisms, and several studies have attempted to combine the MC and phase screen methods for coupled scattering–turbulence propagation [27–31]. Qiao [27] reconstructed phase screen angular spectra via MC-calculated scattering angular spectra and adjusted screen spacing for computational balance; Zhang [28] integrated turbulence, absorption and scattering into a unified MC framework based on the generalized Snell's law for underwater channel analysis; Yang [29] proposed an exponential outer-scale correction model for oceanic turbulence power spectra; Wen [30] combined MC with multi-phase screens to analyze communication performance considering absorption, scattering, and turbulence; Pei [31] optimized phase screen distribution to account for cumulative turbulence effects in multi-screen photon propagation. Despite these advances, existing hybrid models suffer from two critical and common limitations in methodology and research content. Methodologically, these models either ignore coherent optical field interference and superposition [27], neglect phase correlation of photons modulated by different screens [30], or are restricted to forward scattering scenarios unsuitable for large-angle scattering interference analysis [28]. In terms of research content, most studies only output first-order transmission characteristics such as transmittance and energy attenuation, excluding second-order statistical quantities like the scintillation index (SI) [28,30]; a few studies that mention SI lack considerations of interference effects, leading to limited result accuracy [27]. Notably, receiving aperture size, which exerts a critical influence on SI by determining the statistical characteristics of aperture-averaged intensity fluctuations, is rarely addressed in existing hybrid model studies.

SI directly reflects optical field fluctuation severity and serves as a key metric for evaluating transmission stability in complex media [27,29]. Similarly to single-mechanism research, most existing SI analyses focus on scenarios with a single perturbation factor [32,33], while targeted research on composite SI (under combined scattering–turbulence effects) is essential yet scarce for practical atmospheric environments [22,34]. Direct derivation of composite SI from fundamental physical parameters would significantly improve

research efficiency, but current work remains limited to simulation-based verification, lacking analytical quantification methods for composite SI that enable rapid prediction from basic physical parameters. As a core physical quantity describing the energy distribution between scattered and transmitted fields [35,36], the scattered-to-transmitted light intensity ratio determines the composite field interference strength and thus governs composite SI evolution, yet its systematic coupling relationship with composite SI has not been revealed in existing studies.

To address these critical gaps, this paper constructs an atmospheric laser transmission model integrating the MC method and multi-phase screens, with distinct novelties in methodology and content. Methodologically, the model abides by wave optics principles, with the laser field propagating as a complex optical field throughout—entering/exiting the phase screen module in field form, extracting photon coordinates/energy from field intensity distribution for MC scattering, and realizing coherent superposition of scattered spherical wave fields and phase-modulated transmitted fields after each segment, accurately characterizing light field interference coupling. In terms of content, the model takes SI and spatial correlation as core indices, systematically revealing the dynamic competition and nonlinear coupling mechanism between scattering and turbulence in atmospheric environments; it also derives an analytical formula for single-scattering SI from fundamental parameters based on radiative transfer and Mie scattering theories, and it establishes a composite SI expression via the scattered-to-transmitted light intensity ratio, enabling rapid and accurate composite SI calculation.

2. Optical Field Characteristics and Key Features Under Combined Scattering–Turbulence Perturbation

2.1. Simulation Methods for Combined Perturbations and Evolution Characteristics of the Optical Field

In practical atmospheric environments, various discrete scattering particle systems such as smoke, aerosols, water mist, and dust are widely present. Although these particles differ in composition, size, and spatial distribution, they all adhere to the fundamental physical principles governing the interaction between particles and electromagnetic waves. The model constructed in this study is applicable to various discrete scattering particle systems. In this paper, water mist is employed as the medium for investigating particle effects, utilizing a simple droplet particle model that does not account for multimodal particle size distributions or non-spherical characteristics. Mist particles are assumed to be homogeneous in composition and are thus treated as a monodisperse system; their scattering properties are taken as the superposition of scattering effects from particles with different sizes.

To simulate the beam propagation process under the combined effects of particle scattering and turbulence perturbations, this paper adopts a numerical modeling method that alternately combines the Monte Carlo method and the phase screen method to construct a composite transmission simulation model. When employing the Monte Carlo method, the coordinates and energy of incident photons are first sampled according to the intensity distribution across the beam cross-section, using the rejection method to randomly select coordinate and energy values. Subsequently, based on Mie scattering theory, the direction of motion and energy are randomly altered to simulate photon-particle collisions, while simultaneously recording the scattering positions, energy attenuation, and final exit states. Through multiple sampling and result averaging, the optical field distribution and SI are obtained. Starting from the second segment interval, incident information sampling is performed only for the remaining scattered photons. As phase screens do not change

photon coordinates, the spatial positions and energy states of scattered photons at each incidence are consistent with those after transmission through the previous phase screen.

Based on the Huygens–Fresnel principle, the multi-phase screen method is adopted to simulate the phase modulation of the light beam by turbulence. The transmission path is divided into M segments, and the light field on the receiving plane is obtained by evolving the complex amplitude segment by segment. The inverse spectrum method is adopted to generate random phase screens, whose core principle lies in filtering the Gaussian random process based on the refractive index power spectrum of atmospheric turbulence. In this paper, the Von Karman spectrum is selected to characterize the spatial distribution characteristics of atmospheric turbulence, with its expression given as follows [22]:

$$\Phi_n(\kappa) = \frac{0.033C_n^2}{\left(\kappa^2 + \kappa_0^2\right)^{11/6}} \exp(-\kappa^2/\kappa_m^2) \tag{1}$$

where $\boldsymbol{\kappa} = (\kappa_x, \kappa_y, \kappa_z)$ is plane wave vector, $\kappa_m = 2\pi/l_0$, $\kappa_0 = 2\pi/L_0$. In this paper, the light beam propagates along a horizontal path, and C_n^2 is a constant. Meanwhile, the effects of the inner and outer scales of turbulence on the simulation results are not investigated, and their values are kept constant throughout the process.

The filtering function $G(\boldsymbol{\kappa})$ is jointly determined by the Von Karman spectrum and the atmospheric coherence length $r_0 = 0.185\left[\lambda^2 / \int_z^{z+\Delta z} C_n^2(\xi)d\xi\right]^{3/5}$, where z is propagation distance, λ is wavelength, and its form is expressed as follows:

$$G(\kappa) = \left\{0.49\, r_0^{-5/3}\left(\kappa^2 + \kappa_0^2\right)^{-11/6} \exp\left[-\kappa^2/\kappa_m^2\right]\right\}^{1/2} \tag{2}$$

The discrete-form phase screen is obtained by performing the two-dimensional inverse Fourier transform on the filtered Gaussian random process:

$$S(m\Delta x, n\Delta y) = C\sum_{m\prime=0}^{N-1}\sum_{n\prime=0}^{N-1} a(m', n')G(m'\Delta\kappa_x, n'\Delta\kappa_y)\exp\left(\frac{i2\pi mm'}{N} + \frac{i2\pi nn'}{N}\right) \tag{3}$$

where $G(\kappa_x, \kappa_y) = G(\sqrt{\kappa_x^2 + \kappa_y^2})$, $a(m', n')$ is complex Gaussian random variable with unit variance, C is scale factor, and N is resolution. The square receiving plane is divided into a uniform square grid, where N denotes the number of grid cells.

In the model shown in Figure 1, all phase screens are arranged at equal intervals, with their centers aligned along a straight line. The entire transmission path is divided into multiple segments, each of which is simulated sequentially using the combined 'phase screen method + Monte Carlo method'. The composite simulation model strictly follows the wave optics principle, and the laser beam propagates in the form of a complex optical field throughout the whole process. The specific coupling mechanism between the multi-phase screen turbulence model and MC scattering model in each propagation segment is as follows: The complex optical field first enters the multi-phase screen module in field form, and the phase screen modulates the wavefront of the input optical field according to the atmospheric turbulence refractive index distribution, outputting the phase-modulated complex optical field. Then, the field enters the MC scattering module: the MC method first samples and extracts the incident photon coordinates and initial energy according to the intensity distribution of the input complex optical field, and it simulates the random collision and scattering process between photons and aerosol particles based on Mie scattering theory and radiative transfer theory, while recording the scattering position, energy attenuation and final exit state of each photon in real time. After the MC scattering simulation, the

scattered light field (regarded as spherical wave field emitted from scattered particles, with phase and amplitude determined by propagation distance) and the un-scattered transmitted light field are coherently superposed to form the output complex optical field of the current propagation segment. This output optical field then serves as the input optical field of the next propagation segment until the complex optical field propagates to the receiving plane. When the laser field is subjected to these dual disturbances, both its amplitude and phase are simultaneously affected by the random redistribution of energy caused by scattering and the random wavefront distortions induced by turbulence, leading to significant fluctuations. As a core parameter characterizing the intensity of these light fluctuations, SI holds significant engineering application value. Based on this, the present study selects SI as the core quantitative metric, which is expressed as follows [37,38]:

$$SI = \frac{\langle I^2 \rangle}{\langle I \rangle^2} - 1 \tag{4}$$

where $\langle I^2 \rangle$ and $\langle I \rangle$ are both local spatial averages of the light intensity. A small square region is selected at the center of the received optical field to calculate the average light intensity, SI, and the intensity ratio between scattered and transmitted light within this area. The side length of the sampling region is set to one-tenth of the beam waist radius, approximately 0.5 mm. Based on the estimation using the Gaussian intensity distribution formula, the intensity attenuation caused by the beam's radial distribution within this region is less than 3%. Therefore, fluctuations in the incident light intensity are considered negligible, effectively eliminating the interference of the beam's inherent intensity gradient on the local fluctuation characteristics.

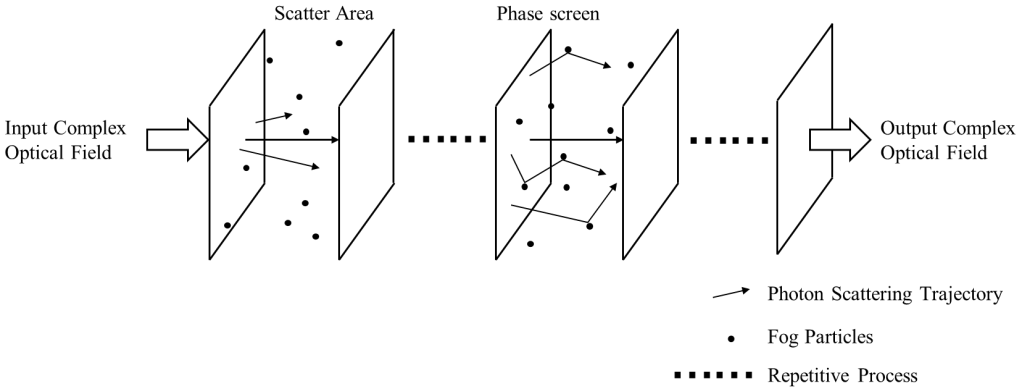

Figure 1. Schematic diagram of the composite simulation algorithm for laser propagation under combined scattering and turbulence effects.

To verify the self-consistency and physical rationality of the proposed coupled MC–multi-phase screen model, limiting case analysis is carried out in this study. When the visibility approaches infinity (scattering effect is negligible), the model is reduced to the classic multi-phase screen turbulence model, and the calculated SI is consistent with the classic turbulence scintillation results; when the Rytov variance is 0 (turbulence effect is negligible), the model is simplified to the pure MC scattering model, and the simulation results of transmittance and SI match the theoretical predictions of Mie scattering and radiative transfer theory. The limiting case analysis confirms the physical soundness of the coupled model, laying a solid foundation for the reliability of the subsequent simulation results.

Based on the fog classification standard of the China Meteorological Administration, the visibility values set in this study cover typical conditions such as light fog, dense fog, and thick fog, with visibility V corresponding to 200 m, 500 m, and 1000 m, respectively. The turbulence intensity includes three typical regimes: weak turbulence, moderate turbu-

lence, and strong turbulence, with Rytov variances σ_I^2 = 0.1, 1, 10, respectively [39]. The number of phase screens is determined under the condition that the propagation between successive screens remains in the weak-fluctuation regime $M > (10\sigma_I^2)^{6/11}$ [40]; the screen spacing must also satisfy the Fresnel-scale requirement $\Delta z < 2L\Delta x/\lambda$ [41]. When the total propagation distance is extended, additional phase screen modules can be simply added while keeping the screen spacing unchanged. Consequently, the inter-screen spacing is set to 80 m, and a total of 12 phase screens are employed, resulting in a total propagation length of 960 m. In this paper, without special annotation in figures, parameters are selected as Table 1. All the above simulation specifications are essential for this study: they ensure the numerical accuracy and statistical stability of the coupled MC–multi-phase screen model, conform to actual atmospheric propagation characteristics, and enable a focused analysis of the core dynamic coupling mechanism between particle scattering and atmospheric turbulence without redundant parameter interference.

Table 1. Parameter selection.

Beam Parameters	Symbols	Value
wavelength	λ	1064 nm
propagation distance	L	960 m
phase screen number	M	12
Gaussian beam waist radius	ω_0	5 mm
phase screen resolution	$N \times N$	1024×1024
side length of phase screen and receiving surface	D	0.3 m
sample number	n	2.5×10^5
inner scale	l_0	1 cm
outer scale	L_0	10 cm

According to the process shown in Figure 2, Figure 3 illustrates the evolution of optical field intensity distribution with propagation distance under different conditions. Under the condition of weak scattering and strong turbulence, the optical field exhibits noticeable random scintillation characteristics as distance increases, with significant intensity fluctuations at the center of the spot. Under the condition of strong scattering and weak turbulence, the optical field demonstrates uniform energy attenuation and blurring, where turbulence-induced scintillation is suppressed by scattering effects, resulting in a smoother spot profile. Under the condition of comparable scattering and turbulence, the optical field simultaneously exhibits both energy attenuation from scattering and fluctuation modulation from turbulence, presenting a unique distribution pattern characterized by coupled attenuation and fluctuation behavior.

Composite SIs are shown in Figure 4. In Figure 4a, the growth rate of the curve initially increases and then decreases, with lower visibility leading to a more pronounced change in the growth rate. In Figure 4b, under strong turbulence, SI first rises and then falls with increasing propagation distance, which originates from the dynamic competition mechanism between turbulence and scattering. The physical essence of the non-monotonic evolution of composite SIs lies in the dynamic transformation of the dominant factor of optical field intensity fluctuations during propagation: In the early propagation stage, the energy of the transmitted light field is dominant, and the random phase distortion caused by atmospheric turbulence leads to the disordered superposition of the optical field

wavefront, which intensifies the local constructive and destructive interference of the light field and thus significantly increases the SI. With the increase in propagation distance, the continuous scattering of aerosol particles depletes the energy of the transmitted light, and the scattered light field with statistical stationarity gradually becomes the main component of the composite light field. The scattered photons follow the Poisson distribution in spatial intensity distribution, and the variance of the intensity fluctuation is equal to the mean value, which makes the SI tend to be stable and converge to 1. In addition, the mutual modulation between scattering and turbulence further amplifies this evolution characteristic: turbulence distorts the photon propagation path, which changes the scattering probability of particles and the energy distribution of scattered light; scattering reduces the energy of the transmitted light field, which weakens the modulation effect of turbulence on the main light field, forming a bidirectional coupling regulation of the scintillation behavior.

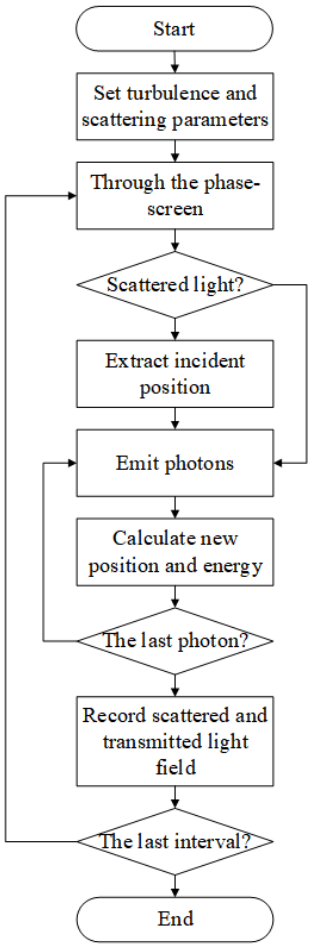

Figure 2. Flowchart of the composite simulation process for coupled model.

Visibility and turbulence intensity regulate the composite SI evolution by changing the energy balance between scattered and transmitted light and the degree of optical field wavefront distortion, respectively. For different visibility conditions, lower visibility means higher aerosol particle number density and stronger scattering effect, which accelerates the energy attenuation of the transmitted light field and makes the scattered light field become dominant in a shorter propagation distance. Thus, the SI peak appears earlier and the peak value is smaller. Higher visibility weakens the scattering effect, the transmitted light field maintains the energy advantage for a longer time, and the turbulence perturbation can be fully developed, leading to a higher SI peak and a later occurrence position. For different turbulence intensity conditions, stronger turbulence leads to more severe random phase

distortion of the optical field, which significantly enhances the interference fluctuation of the transmitted light field in the early propagation stage and thus increases the SI peak value; at the same time, strong turbulence accelerates the energy dissipation of the transmitted light field through path deflection, making the scattered light field dominant in advance, so the SI peak appears earlier. The synergistic regulation of the two factors forms the diverse evolution characteristics of composite SI under different atmospheric conditions.

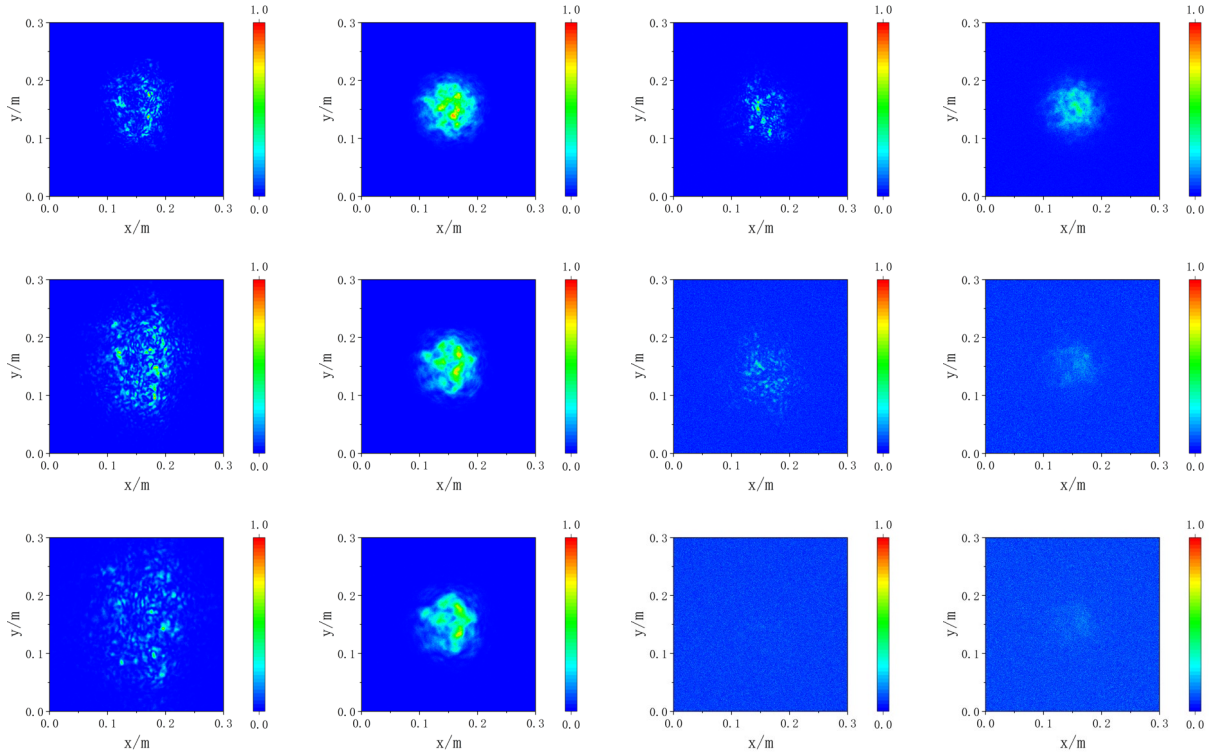

Figure 3. Spatial intensity distribution of Gaussian laser beams under different atmospheric scattering–turbulence combinations and propagation distances (160 m, 320 m, 480 m for rows; strong turbulence–high visibility, weak turbulence–high visibility, strong turbulence–low visibility, weak turbulence–low visibility for columns).

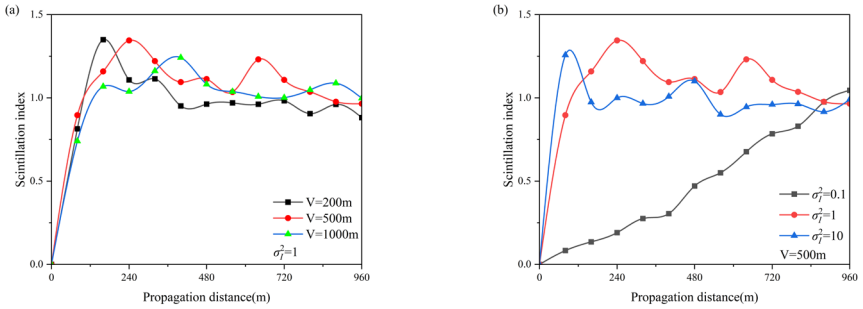

Figure 4. Variation in composite scintillation index (SI) with propagation distance under combined scattering–turbulence effects. (**a**) Varying with visibility; (**b**) varying with turbulence strength.

By continuously moving the position of the square sampling region on the receiving plane, the variation curve of spatial correlation is obtained, as shown in Figure 5. All curves exhibit a two-stage characteristic: an initial sharp decline followed by a relatively moderate decrease. The first stage of sharp decline is primarily dominated by short-range intense turbulence disturbances, where the rapid wavefront distortion caused by turbulence leads to a swift breakdown of coherence within small spatial scales. The more gradual decline in the second stage reflects the long-range statistical effects of scattering, as the

random distribution of scattered photons exhibits a smoother influence over larger spatial scales. The final stabilized values of some curves are greater than zero, and this value gradually decreases as visibility decreases or turbulence intensity increases, due to the residual coherence in the optical field that is never entirely destroyed. Overall, lower visibility or higher turbulence intensity leads to a faster decay in the spatial correlation of the optical field. High particle concentrations along the propagation path increase the probability of photon-particle collisions, altering the direction of a large number of photons. The random motion of scattered photons breaks the intensity correlation of the originally spatially coherent optical field at different spatial positions. Turbulence causes an irregular spatial distribution of atmospheric refractive index, imposing random phase distortions on the optical field and thereby disrupting its spatial coherence.

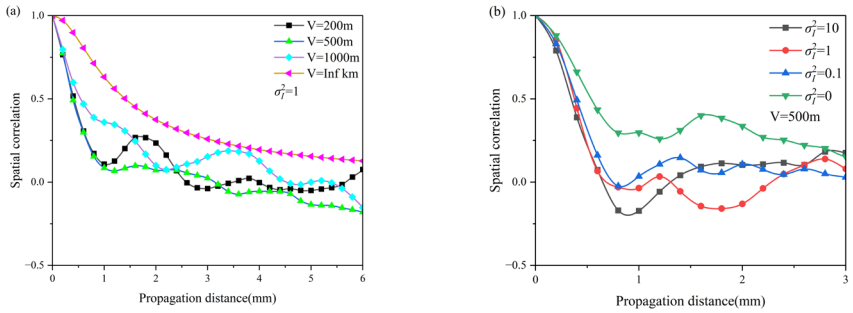

Figure 5. Variation in optical field spatial correlation with propagation distance under combined scattering–turbulence effects. (**a**) Varying with visibility; (**b**) varying with turbulence strength.

2.2. Light Intensity Ratio and Its Relationship with SI

The two simulation methods influence the amplitude, phase, and energy distribution of scattered and transmitted light through different mechanisms. Therefore, the relative variation between the scattered and transmitted components of a Gaussian beam during propagation is a key factor leading to changes in the beam's transmission characteristics under perturbations. This relative variation between scattered and transmitted light can be characterized by their intensity ratio, which is defined as

$$r = \frac{I_s}{I_t} \tag{5}$$

where I_s is the scattered light intensity and I_t is the transmitted light intensity. The transmittance at different distances under varying visibility conditions is shown in Figure 6. The variation curve of r is presented in Figure 7.

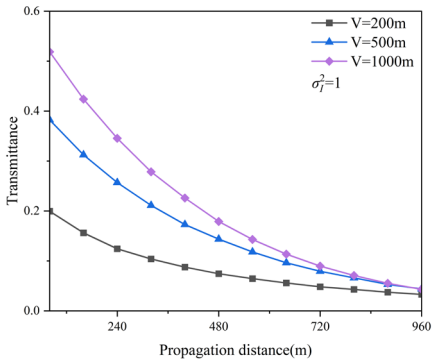

Figure 6. Variation in laser transmittance with propagation distance under different visibility conditions.

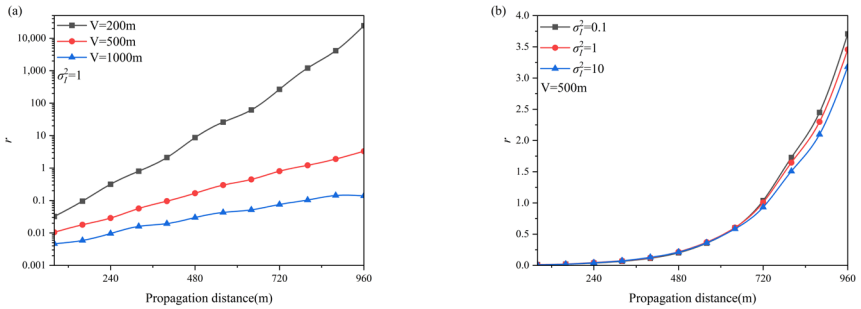

Figure 7. Variation in scattered-to-transmitted light intensity ratio with propagation distance under combined scattering–turbulence effects. (**a**) Varying with visibility; (**b**) varying with turbulence strength.

From Figure 6, it can be observed that as the transmission distance increases, the transmittance under all visibility conditions shows a continuous declining trend. Especially when the transmission distance approaches 960 m, the transmittance has dropped to an extremely low level, indicating that the energy proportion of the transmitted light is negligible at this point. The attenuation is essentially determined by the scattering optical thickness τ, and its relationship with visibility is given by $\tau = 3.912/V$. Simulation results reveal that the transmittance under combined perturbations deviates from the theoretical value for pure scattering. This discrepancy arises from the modulation of photon paths by turbulent phase perturbations: some photons that initially deviate from the detection region are redirected and recollected due to turbulence-induced deflection, while some focused photons are scattered out of the detection field by turbulence. This visually demonstrates the coupling effect between scattering and turbulence.

From Figure 7, it can be seen that both visibility and turbulence intensity significantly regulate the light intensity ratio. Under low visibility, r increases logarithmically; under high visibility, the scattering effect of particles is weak, and r grows slowly. Compared with Figure 6, when the transmittance is extremely low, the energy of the transmitted light approaches zero. The relative proportion of scattered light energy causes r to become extremely large due to the sharp decrease in transmitted light energy. At this point, r can no longer effectively reflect the relationship between the scattered and transmitted optical fields, and its reference significance is limited. The differences in the variation in r under different visibility conditions stem from the high particle density under low visibility, where scattering consumes the energy of transmitted light more intensely, leading to an exponential increase in the relative proportion of scattered light intensity. Under high visibility, particles are sparse, the energy consumption effect of scattering is weak, and the energy advantage of transmitted light is maintained over a longer period. The greater the turbulence intensity, the stronger its effect on the phase distortion and energy dissipation of transmitted light, indirectly accelerating the energy conversion from transmitted light to scattered light, thereby making the relative proportion of scattered light intensity increase more significantly.

To investigate how r affects the variation in the composite SI, we start from the definition of SI and derive a calculation formula that includes r. Based on the uncorrelated superposition of the scattered and transmitted fields, the composite SI can be expressed as

$$SI = \frac{\mathrm{var}(I_s) + \mathrm{var}(I_t)}{(\mu_s + \mu_t)^2} \tag{6}$$

where $\mu_s = \langle I_s \rangle$ and $\mu_t = \langle I_t \rangle$ are the local spatial average intensities of the scattered and transmitted light, respectively.

For the scattered light $SI_s = \mathrm{var}(I_s)/\mu_s$ and for the transmitted light $SI_t = \mathrm{var}(I_t)/\mu_t$. Substituting these into the above equation yields

$$SI = \frac{\mu_s^2 \times SI_s + \mu_t^2 \times SI_t}{(\mu_s + \mu_t)^2} \tag{7}$$

Substituting r into Equation (7), we finally obtain the method to calculate the composite SI using only information from the scattered and transmitted fields:

$$SI = \frac{r^2 \times SI_s + SI_t}{(r+1)^2} \tag{8}$$

Comparing the results calculated by Equation (7) with those presented in Figure 4 yields the difference between the two methods, as illustrated in Figure 8.

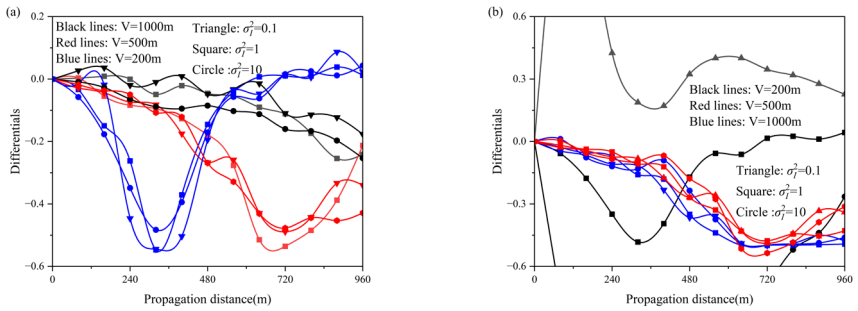

Figure 8. Differentials between results calculated by Equation (7) and composite SI of all 9 combinations of visibility (200 m/500 m/1000 m) and Rytov variance (0.1/1/10). (**a**) Varying with visibility; (**b**) varying with turbulence strength.

From Figure 8a, it can be observed that the maximum/minimum values, extreme points, and periods of each differential curve are different, showing a clear periodic fluctuation characteristic that aligns with the shape of a sinusoidal function. The curve characteristics are related to visibility: the extreme points shift backward as visibility increases, the period increases with visibility, and the amplitude is around 0.5. Therefore, a sinusoidal compensation term is constructed, with visibility and propagation distance as variables. It is observed that the half-period is $V/100 + 2$. Allowing for a certain error margin, each curve has a phase shift, calculated to be $8V/1000$. Thus, the final constructed compensation term is

$$\mathrm{Jia}_v = 0.5 \times \sin\left[\frac{\pi}{2v}\left(\frac{l}{100} - 0.8v\right)\right] \tag{9}$$

From Figure 8b, it can be seen that the differential curves exhibit a concentrated trend, showing a monotonic change similar to a logarithmic function. Therefore, a logarithmic compensation term is constructed as

$$\mathrm{Jia}_c = 0.1 \times \log_2\left(\frac{l}{100}\right) \tag{10}$$

To fully characterize the deviation characteristics, we supplement the simulation analysis of all 9 combinations of visibility and Rytov variance. From the full set of deviation data, we summarize two typical and stable trends: the deviation curves along the visibility dimension maintain regular sinusoidal fluctuations under $V \geq 500$ m, while the deviation curves along the turbulence intensity dimension present stable monotonic logarithmic variation under all visibility conditions. However, the deviation data under $V = 200$ m lose the above regular characteristics and show severe irregular fluctuations, and direct numerical simulation of the coupled MC-multi-phase screen model is still required to

obtain reliable composite SI results. The deep physical mechanisms underlying the specific sinusoidal and logarithmic deviation trends summarized from the data remain to be further investigated—this is due to the complex nonlinear coupling between aerosol multiple scattering, turbulence phase modulation, and coherent optical field interference in the atmospheric channel, which involves the joint action of multiple microscopic physical processes that need more refined modeling to explore.

The compensation terms are added to SI calculated from the intensity ratio of scattered to transmitted light, yielding the coupled SI, as shown in Figure 9.

$$SI_{total} = SI + \text{Jia} \tag{11}$$

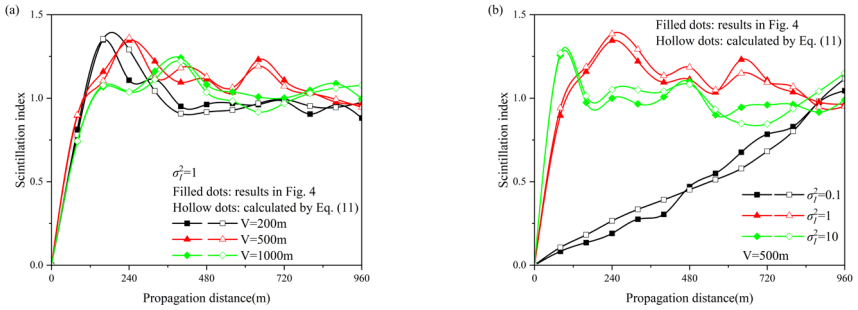

Figure 9. Comparison of composite SI between compensated analytical results from Equation (11) and direct simulation results under combined scattering–turbulence effects. (**a**) Varying with visibility; (**b**) varying with turbulence strength.

As can be seen from the figure, the coupled results are in close agreement with the composite simulation results. During the simulation process, inevitable light intensity variations within a finite region introduce additional SI. The difference along the visibility dimension exhibits periodic fluctuations, consistent with a sinusoidal function shape, due to the periodic nature of phase interference between scattered and transmitted light. The difference along the turbulence intensity dimension shows a monotonic variation, aligning with a logarithmic function shape, owing to the cumulative effects of energy dissipation caused by turbulence and the associated quantization errors.

3. Coupling Relationship of Single-Perturbation SIs

3.1. Derivation of Formulas for Calculating SIs from Basic Parameters

Direct composite simulation of the optical field or the use of Monte Carlo methods typically involves cumbersome procedures, complex parameter settings, and time-consuming computations. To rapidly assess the variation patterns of light beams under combined effects, this paper derives a formula for calculating SIs based on fundamental parameters in the presence of particle scattering alone. It further seeks to establish the relationship through which this result couples with SI obtained using the phase screen method for turbulence-only scenarios to yield the composite SI. Since simulating beam propagation through turbulence using the phase screen method requires very short computation times, SI can be quickly obtained directly via the phase screen approach when only turbulence is present.

Multiple scattering causes the intensity fluctuations to follow a log-normal distribution, meaning the natural logarithm of the intensity obeys a normal distribution. The variance of this log-normal distribution, $\sigma^2_{\ln I}$, is the core quantity related to SI. The relationship between $SI_{scar\text{-}only}$ and $\sigma^2_{\ln I}$ is

$$SI_{\text{scar}-\text{only}} = \sqrt{\exp(\sigma^2_{\ln I}) - 1} \tag{12}$$

The log-variance [30] is contributed by the fluctuations of both the collimated and diffuse light. It is necessary to derive the log-variance for each component separately and then calculate the total log-variance, while considering the statistical properties of incoherent superposition. For the transmitted light component, whose intensity follows a Poisson distribution due to the randomness of photon propagation and scattering [42], the log-variance satisfies

$$\sigma^2_{\ln It} = \exp(\rho\sigma_t z) \tag{13}$$

where ρ is the particle number density, σ_t is the total particle cross-section.

The scattered light component is composed of the superposition of a large number of multiply-scattered photons. The log-variance of its intensity fluctuation is positively correlated with the average number of scattering events [30,42]. According to the diffusion approximation of radiative transfer theory [42], the log-variance of the scattered light can be expressed as

$$\sigma^2_{\ln Is} = \alpha \times [1 - \exp(\rho\sigma_t z)] \tag{14}$$

where α is the multiple scattering log-variance coefficient, related to the asymmetry factor g calculated from Mie scattering theory:

$$\alpha \propto \frac{1}{1 - \langle g \rangle} \tag{15}$$

where $\langle g \rangle$ is the scattering cross-section weighted average of the asymmetry factor for particles of different sizes

$$\langle g \rangle = \frac{\sum_{i=1}^{N} g_i \cdot \sigma_{sca,i} \cdot N_r(i) \cdot dr}{\sum_{i=1}^{N} \sigma_{sca,i} \cdot N_r(i) \cdot dr} \tag{16}$$

where σ_{sca} is the particle scattering cross-section, N_r is the particle size distribution function, and dr is the size step.

The total log-variance is the intensity-weighted sum of their respective log-variances:

$$\sigma^2_{\ln I} = \frac{\langle I_s \rangle}{\langle I \rangle}\sigma^2_{\ln I_s} + \frac{\langle I_t \rangle}{\langle I \rangle}\sigma^2_{\ln I_t} \tag{17}$$

For a scenario involving only particle scattering, the total intensity at the receiver plane is formed by the incoherent superposition of the collimated light I_t and the scattered light I_s. According to the first-order multiple scattering approximation of radiative transfer [42], the transmitted light intensity follows exponential attenuation:

$$\langle I_t \rangle = I_0 \times \exp(-\rho\sigma_t z) \tag{18}$$

where I_0 is the incident intensity, z is propagation distance. Substituting $\langle I \rangle = \langle I_s \rangle + \langle I_t \rangle = I_0$ and simplifying yields

$$\sigma^2_{\ln I} = 1 + \alpha \times [1 - \exp(\rho\sigma_t z)]^2 \tag{19}$$

Substituting the total log-variance into the relationship between SI and the log-variance gives

$$SI_{\text{scar}-\text{only}} = \sqrt{\exp(1 + \alpha \times [1 - \exp(\rho\sigma_t z)]^2 - 1)} \tag{20}$$

3.2. Verification of Single-Factor Perturbation Simulation and Coupling Relationship

Substituting the fundamental parameters into Equation (20), the variation in SI under scattering alone is calculated and compared with the results obtained from running the

Monte Carlo method independently, as shown in Figure 10. Since processes such as coordinate and energy sampling, as well as the setting of motion direction and step length in the Monte Carlo method, involve stochastic operations, the following averaging strategy is adopted in this paper to reduce simulation errors: each simulation is configured with an incident photon count of 2.5×10^5, and the results are averaged over three independent runs.

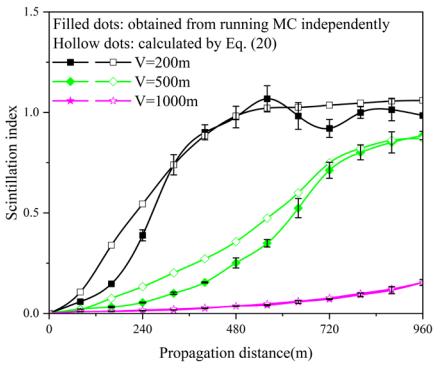

Figure 10. Comparison of single-scattering SI between analytical results from Equation (20) and independent MC simulation results at different visibility.

Error bars for all data points are calculated from the standard deviation of the corresponding statistical results. Overall, the fluctuation amplitude is small, with a maximum relative error of less than 15%, indicating that the Monte Carlo simulation sample size of 250,000 photons adopted in this study is sufficient to effectively suppress statistical noise and ensure the stability and reliability of the results. The SI curve calculated based on Equation (20) is smooth and regular, whereas the simulation results obtained using the Monte Carlo method exhibit minor fluctuations due to detailed differences in the optical field under random scattering and turbulence perturbations. Nevertheless, the two show good agreement in terms of growth trend, peak location, and final stable value, demonstrating that the proposed fundamental parameter calculation method has good reliability under conditions of moderate turbulence intensity. However, despite the good consistency between the fundamental parameter calculation method and simulation results in weak turbulence scenarios, limitations still exist under severe conditions.

Comparing SI obtained from separately running Monte Carlo and phase screen simulations for single perturbations with the composite SI in Figure 4, it is found that the two cannot be simply coupled to yield the composite SI. We directly examined the relationship among the three curves and discovered the following relationship:

$$SI = (SI_{scar-only} + SI_{turb-only}) - SI_{scar-only} \times SI_{turb-only} \tag{21}$$

Substituting the simulated SI into Equation (21) yields the results shown in Figure 11. It can be observed from the figure that the coupled results match those in Figure 4, indicating that the method of coupling after independent simulations can effectively reproduce the scintillation characteristics of the beam under combined effects.

For a more intuitive analysis, Equation (21) is transformed into

$$SI = SI_{scar-only} \times (1 - SI_{turb-only}) + SI_{turb-only} \tag{22}$$

The successful establishment of this coupling formula demonstrates that the composite SI is not a simple linear superposition of the two effects, but rather a nonlinear coupling through a form involving the factor $(1 - SI)$. This mathematically quantifies the competitive relationship between the two effects, where the weakening of one leads to the strengthening of the other. The coupling formula can reflect both the synergistic reinforcement of the

two mechanisms and their dynamic seesaw relationship. The scintillation contribution from the scattering mechanism is proportionally weakened by the action of the phase screen mechanism, and conversely, the scintillation contribution from the phase screen mechanism is partially offset by the presence of the scattering mechanism. Analyzing the physical process, the phase perturbation from turbulence alters the interference conditions of the scattered light, thereby suppressing the scintillation effect of scattering. Meanwhile, as the propagation distance increases, the rising proportion of scattered light intensity reduces the energy of the transmitted light, consequently diminishing the target for turbulence perturbation and leading to a weakened scintillation contribution from turbulence. Under extremely low visibility and extremely weak turbulence, the formula simplifies to the scattering-dominated SI; under extremely high visibility and extremely strong turbulence, it simplifies to the turbulence-dominated SI. By quantifying this nonlinear relationship, a numerical match with the direct composite field results is achieved, validating the conclusion that the combined effect of particle scattering and turbulence perturbation is not a simple linear superposition.

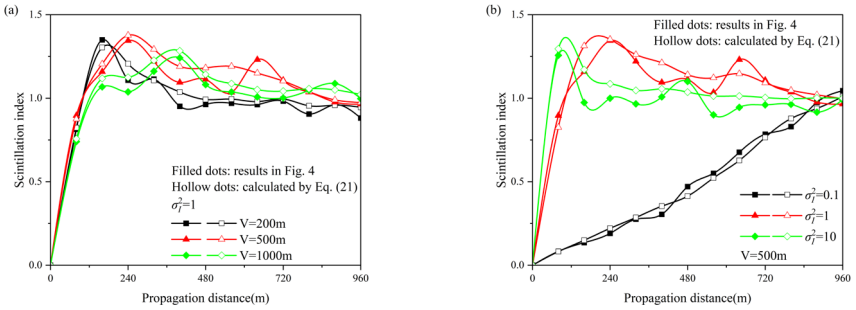

Figure 11. Comparison of composite SI between coupling analytical results from Equation (21) and direct simulation results under combined scattering–turbulence effects. (**a**) Vary with visibility. (**b**) Vary with turbulence strength.

4. Conclusions

This paper systematically investigates the propagation characteristics of Gaussian beams under the combined effects of particle scattering and atmospheric turbulence. Through theoretical derivations and numerical simulations, the physical mechanisms governing intensity fluctuations in the composite optical field are revealed, and the coupling relationships among key parameters are established.

A numerical simulation model of the composite optical field based on the phase screen method and the Monte Carlo method was established, and the variation in SI with propagation distance under different visibility and turbulence intensity conditions was obtained. The results show that SI exhibits a characteristic pattern of first increasing and then decreasing, which fundamentally stems from the dynamic interplay between turbulence perturbation and particle scattering during propagation. In the initial stage of propagation, strong perturbations by turbulence intensify the light intensity fluctuations, driving SI upward. As the propagation distance increases, the energy proportion of scattered light gradually rises, causing SI to eventually stabilize. Under high-visibility conditions, the attenuation of transmitted light is slower, allowing turbulence effects to fully develop, resulting in a significantly higher peak SI compared to low-visibility scenarios. For a fixed visibility, stronger turbulence leads to a higher peak SI and an earlier occurrence of this peak.

Based on the definition of SI, this paper derives a theoretical formula for directly calculating the composite SI using the intensity ratio of scattered to transmitted light. To address the systematic deviation between the results computed by this formula and those

from direct composite optical field simulations, a compensation mechanism is introduced based on the physical characteristics of the deviation curves. The validated, compensated model can accurately simulate the composite field SI using only information from the scattered and transmitted fields.

A clear analytical calculation pathway for SI under single-scattering effects has been established. Based on radiative transfer theory and Mie scattering theory, a direct mapping from microscopic particle parameters and macroscopic medium parameters to SI is achieved, leading to the derivation of a closed-form expression that quantifies the nonlinear relationship between scattering intensity and SI. The study reveals that the composite SI is not a simple superposition of the results from the two individual effects, indicating the existence of competition and coupling mechanisms between scattering and turbulence, which jointly influence scintillation behavior.

By establishing numerical simulation methods, identifying coupling relationships, and analyzing physical mechanisms, this study provides an effective reference for simulating and predicting laser propagation characteristics in complex atmospheric environments. In future works, we will explore the deep physical mechanisms of the observed deviation trends and establish a rigorous physical correction framework to replace the empirical compensation terms. It is essential to break through the current model's limitations under extreme atmospheric conditions, realize accurate prediction of laser transmission characteristics in all actual atmospheric scenarios, and further provide more reliable theoretical and technical support for the engineering application of laser communication, remote sensing and lidar systems in complex atmospheric environments.

Author Contributions: Conceptualization, L.W. and Y.Y.; Methodology, L.W. and Y.Y.; Software, L.W. and Y.Y.; Validation, L.W. and Y.Y.; Formal analysis, L.W. and Y.Y.; Investigation, Y.Y.; Resources, Y.Y.; Data curation, Y.Y.; Writing—original draft, Y.Y.; Writing—review & editing, Y.Y.; Visualization, Y.Y. and L.G.; Supervision, L.G.; Project administration, L.G.; Funding acquisition, L.G., W.W., Z.Y., L.Y. and Y.L. All authors have read and agreed to the published version of the manuscript.

Funding: This research was funded by National Natural Science Foundation of China (No. 62201566), Natural Science Basic Research Program of Shaanxi Province (No. 2025JC-YBMS-082), and Natural Science Foundation of Shaanxi Province (No. 2025JC-YBMS-744).

Data Availability Statement: Data underlying the results presented in this paper may be obtained from the authors upon reasonable request.

Conflicts of Interest: The authors declare no conflicts of interest.

References

1. Yeh, C.; Chen, J.; Chen, H. Selectable dual-wavelength erbium-doped fiber laser with stable single-longitudinal-mode utilizing eye-type compound-ring configuration. *Opt. Laser Technol.* **2016**, *82*, 72–75. [CrossRef]
2. Midwinter, J.E. Progress in optical communication. *Opt. Laser Technol.* **1981**, *13*, 49–51. [CrossRef]
3. Wang, J.; Lv, J.; Zhao, G. Free-space laser communication system with rapid acquisition based on astronomical telescopes. *Opt. Express* **2015**, *23*, 20655–20667. [CrossRef]
4. Popoola, W.O.; Ghassemlooy, Z.; Lee, C.G. Scintillation effect on intensity modulated laser communication systems—A laboratory demonstration. *Opt. Laser Technol.* **2010**, *42*, 682–692. [CrossRef]
5. Xu, C.; Zha, B.; Zhang, R. Echo characteristics of pulsed lasers in non-uniform smoke environments. *Opt. Express* **2024**, *32*, 24222–24241. [CrossRef]
6. Barcik, P.; Wilfert, O.; Dobesch, A. Experimental measurement of the atmospheric turbulence effects and their influence on performance of fully photonic wireless communication receiver. *Phys. Commun.* **2018**, *31*, 212–217. [CrossRef]
7. Xu, F.; He, X.; Shanmugam, P. Effects of the Earth curvature on Mie-scattering radiances at high solar-sensor geometries based on Monte Carlo simulations. *Opt. Express* **2024**, *32*, 6706–6732. [CrossRef] [PubMed]
8. Wang, C.; Philpot, W.; Kim, M. A Monte Carlo study of the seagrass-induced depth bias in bathymetric lidar. *Opt. Express* **2011**, *19*, 7230–7243. [CrossRef] [PubMed]

9. Premuda, M.; Palazzi, E.; Ravegnani, F. MOCRA: A Monte Carlo code for the simulation of radiative transfer in the atmosphere. *Opt. Express* **2012**, *20*, 7973–7993. [CrossRef]
10. Wang, L.; Jacques, S.L.; Zheng, L. MCML—Monte Carlo modeling of light transport in multi-layered tissues. *Comput. Methods Programs Biomed.* **1995**, *40*, 131–146. [CrossRef]
11. Wang, G. *Research on Transmission Characteristics of Laser under Complex Atmospheric Background*; Xidian University: Xi'an, China, 2007; pp. 66–71.
12. Wang, H.; Sun, H.; Song, Z. Numerical calculation and analysis of transmittance of smoke screen based on Monte Carlo method. *Infrared Laser Eng.* **2012**, *41*, 1200–1205.
13. He, L.; Duan, J.; Zhang, S. Simulation of Polarization Transmission Characteristics of Laser in Sea Fog Environment. *Laser Optoelectron. Prog.* **2021**, *58*, 0329001. [CrossRef]
14. Rakovic, M.; Kattawar, G.; Mehrubeoglu, M. Light backscattering polarization patterns from turbid media: Theory and experiment. *Appl. Opt.* **1999**, *38*, 3399–3408. [CrossRef] [PubMed]
15. van der Laan, J.D.; Wright, J.B.; Kemme, S.A. Superior signal persistence of circularly polarized light in polydisperse, real-world fog environments. *Appl. Opt.* **2018**, *57*, 5464–5473. [CrossRef]
16. Qian, X.; Zhu, W.; Rao, R. Numerical investigation on propagation effects of pseudo-partially coherent Gaussian Schell-model beams in atmospheric turbulence. *Opt. Express* **2009**, *17*, 3782–3791. [CrossRef]
17. Xiang, J. Accurate compensation of the low-frequency components for the FFT-based turbulent phase screen. *Opt. Express* **2012**, *20*, 681–687. [CrossRef] [PubMed]
18. Vetelino, F.; Young, C.; Rews, L. Aperture averaging effects on the probability density of irradiance fluctuations in moderate-to-strong turbulence. *Appl. Opt.* **2017**, *46*, 2099–2108. [CrossRef] [PubMed]
19. Vorontsov, M.; Lachinova, S.L.; Vorontsov, M.A. Optimization of Turbulence Phase Screen Distribution for Wave-Optics Analysis of Laser Beam Propagation over Extended-Range Atmospheric Paths. In *Imaging and Applied Optics Congress*; Optica Publishing Group: Washington, DC, USA, 2020; p. JW5B.5.
20. Wu, H.; Yan, H.; Li, X. Statistical interpolation method of turbulent phase screen. *Opt. Express* **2009**, *17*, 14649–14664. [CrossRef]
21. Qian, X.; Zhu, W.; Rao, R. Phase screen distribution for simulating laser propagation along an inhomogeneous atmospheric path. *Acta Phys. Sin.* **2009**, *58*, 6633–6639. [CrossRef]
22. Wang, L. Characteristics of Laser Beam Target Echo in Turbulent Atmosphere. Ph.D. Thesis, Xidian University, Xi'an, China, 2014.
23. Feng, F. Simulation of Atmospheric Turbulence Phase Screen Based on Wavelet Analysis. *Acta Opt. Sin.* **2007**, *37*, 0101004. [CrossRef]
24. Zhang, D.; Chen, Z.; Xiao, C. Generation of High-precision Turbulence Phase Screen Based on Modified Atmosphere Spectrum. *Acta Photonica Sin.* **2020**, *49*, 0601002. [CrossRef]
25. Yang, Y.; Gong, Y.; Leng, K. A simulation scheme of high power laser atmospheric transmission based on complex phase screen. *Laser Infrared* **2021**, *51*, 415–420.
26. Geng, X.; Liu, Z.; Li, W. Study on the Propagation Characteristics of Lasers in Dynamic Atmospheric Turbulence. *Laser Infrared* **2024**, *54*, 40–47.
27. Zhang, J.; Kou, L.; Yang, Y. Monte-Carlo-based optical wireless underwater channel modeling with oceanic turbulence. *Opt. Commun.* **2020**, *475*, 126214. [CrossRef]
28. Qiao, M.; Yuan, X. Realistic phase screen model for forward multiple-scattering media. *Opt. Lett.* **2020**, *45*, 1031–1034. [CrossRef] [PubMed]
29. Yi, Y.; Huan, N.; Xiao, W. Influence of Outer Scale of Ocean Turbulence on Propagation Characteristics of Gaussian Beams. *Acta Photonica Sin.* **2023**, *52*, 0401002.
30. Wen, H.; Yin, H.; Ji, X. Modeling and performance analysis of underwater wireless optical absorption, scattering, and turbulence channels employing Monte Carlo-multiple phase screens. *Appl. Opt.* **2023**, *62*, 6883–6891. [CrossRef]
31. Pei, K. *Research on Optical Wireless Transmission Characteristics and Simulation Platform Design in Complex Marine Environments*; Guilin University of Electronic Technology: Guilin, China, 2024.
32. Andrews, L.C. Beam Wander and the Scintillation Index. In *Optical Sensors and Sensing Congress*; Optica Publishing Group: Washington, DC, USA, 2020.
33. Jia, R.; Wei, H.Y.; Zhang, H. Scintillation index of echo wave in slant atmospheric turbulence. *Optik* **2015**, *126*, 5122–5126. [CrossRef]
34. Jenu, M.; Bebbington, D. Intensity scintillation index of finite beam optical propagation in a turbulent atmosphere. *Electron. Lett.* **1994**, *30*, 582–583. [CrossRef]
35. Koňák, Č.; Jakeš, J.; Štěpánek, P. Effect of multiple light scattering on transmitted and scattered light. *Appl. Opt.* **1991**, *30*, 4865–4871. [CrossRef]
36. Qi, H.; Liu, D.; Chen, Z. Study on the effects of atmospheric environment on the transmittance of laser transmission based on the Monte Carlo method. In *AOPC 2021*; SPIE Press: Bellingham, WA, USA, 2021.

37. Korotkova, O.; Farwell, N.; Shchepakina, E. Light scintillation in oceanic turbulence. *Waves Random Complex Media* **2012**, *22*, 260–266. [CrossRef]
38. Andrews, L.C.; Phillips, R.L.; Hopen, C.Y. *Laser Beam Scintillation with Applications*; SPIE Press: Bellingham, WA, USA, 2001; Volume 99.
39. Cheng, M. *Propagation of Structured Beams Through Typical Turbulent Environment*; Xidian University: Xi'an, China, 2018.
40. Knepp, D. Multiple phase-screen calculation of the temporal behavior of stochastic waves. *Proc. IEEE* **1983**, *71*, 722–737. [CrossRef]
41. Flatté, M.; Gerber, J. Irradiance-variance behavior by numerical simulation for plane-wave and spherical-wave optical propagation through strong turbulence. *J. Opt. Soc. Am. A* **2000**, *17*, 1092–1097. [CrossRef] [PubMed]
42. Guo, L.; Zhang, M.; Wu, Z. *The Basic Theory and Methods of Composite Electromagnetic Scattering of Random Rough Surfaces and Targets*; Science Press: Beijing, China, 2014.